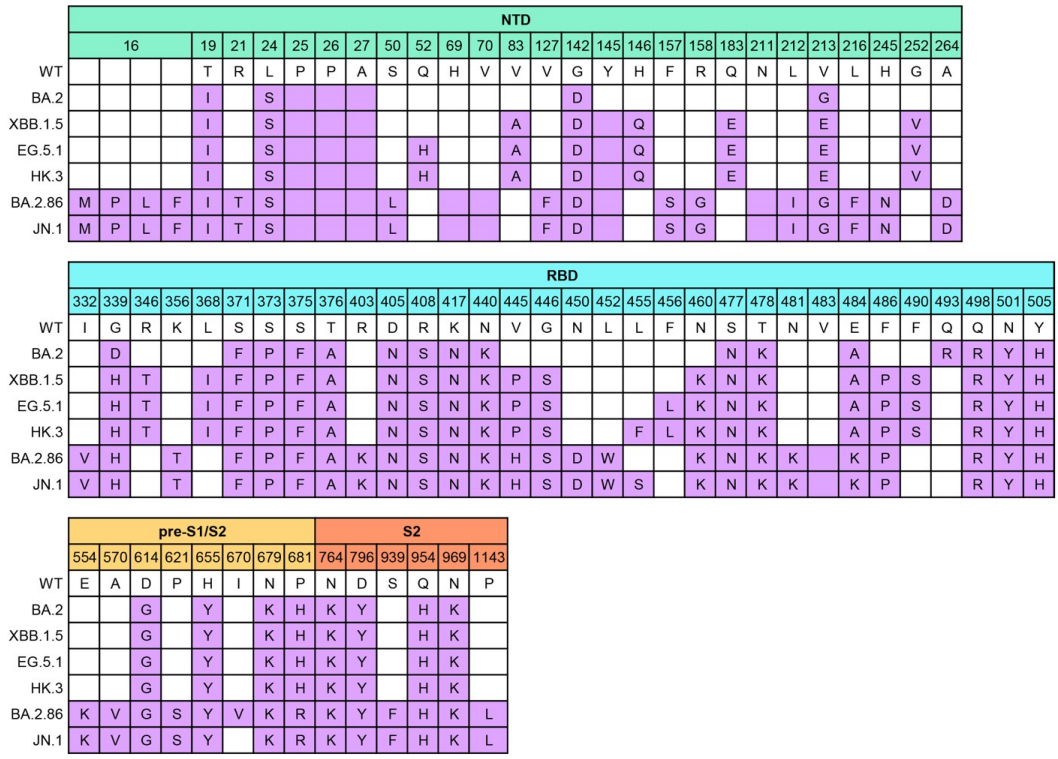

Fig. S1. Key amino acid mutations in the spike protein were identified in Omicron subvariants.

Amino acid substitutions were marked in purple and deletions were marked by purple spaces.

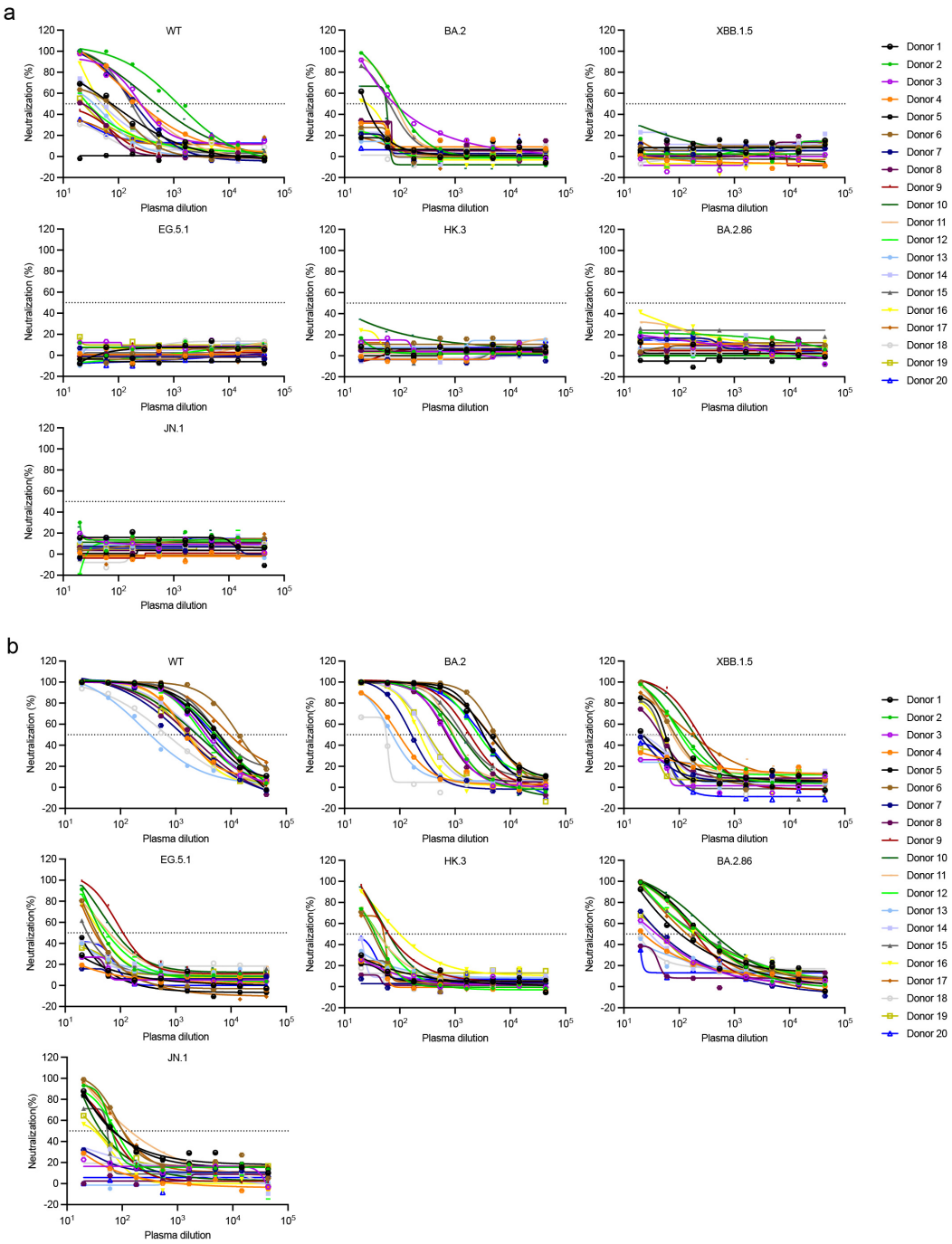

Fig. S2. Neutralization curves of plasma samples collected from BA.4 or BA.5 breakthrough infections at Visit 1 (a) and Visit 2 (b) against various SARS-CoV-2 variants.

The neutralization curves of one out of two independent experiments with similar results were displayed and a cut-off value of 50% in neutralization was indicated by the dotted horizontal line. Source data are provided as a Source Data file.

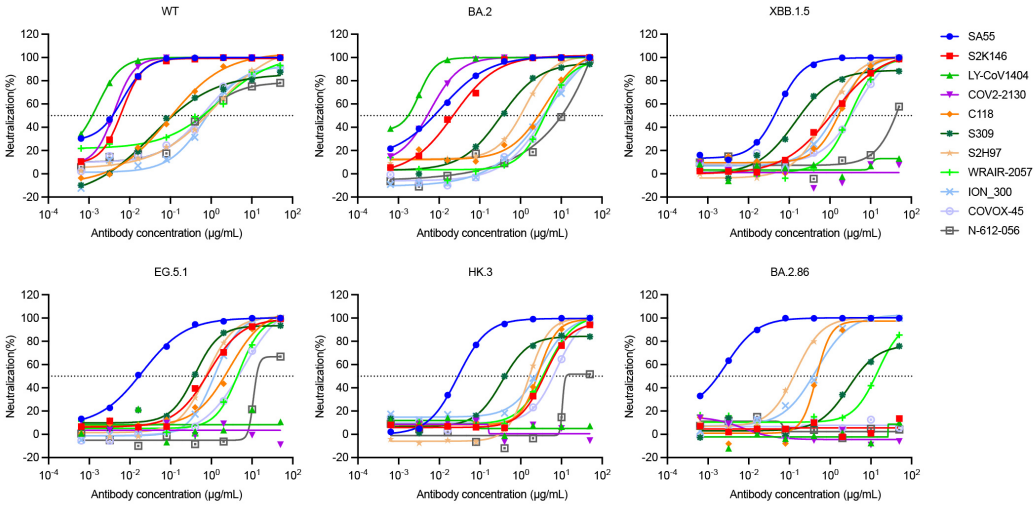

Fig. S3. Neutralization curves of RBD-specific broadly neutralizing mAbs against various SARS-CoV-2 variants.

The neutralization curves of one out of two independent experiments with similar results were showed and a cut-off value of 50% in neutralization was indicated by the dotted horizontal line. All mAbs were serially 5-fold diluted from the highest concentration of 50 ug/mL to a total of 8 dilutions. Source data are provided as a Source Data file.

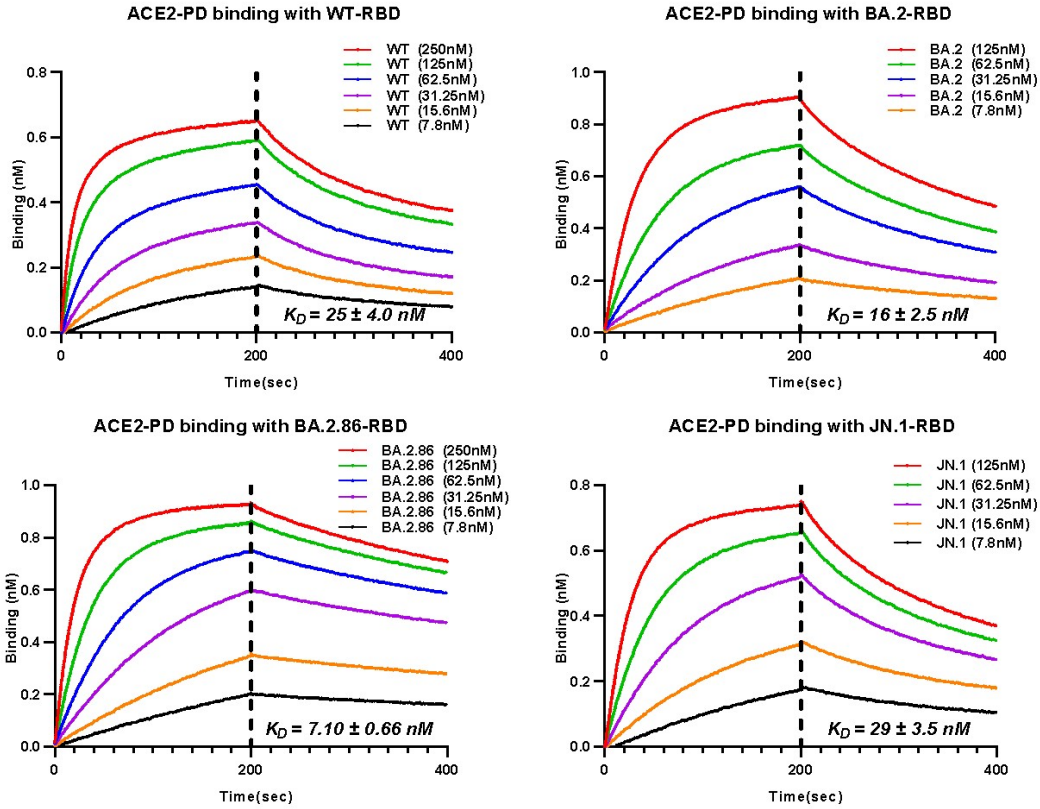

Fig. S4. The different affinities of multiple SARS-CoV-2 subvariants with the host receptor ACE2.

Binding affinities of the S-RBD from different Omicron subvariants with the peptidase domain of ACE2 (ACE2-PD). The association and dissociation of S-RBD, applied at different concentrations, with biotinylated ACE2 PD-liganded SA biosensors were measured using Biolayer Interferometry (BLI). Source data are provided as a Source Data file.

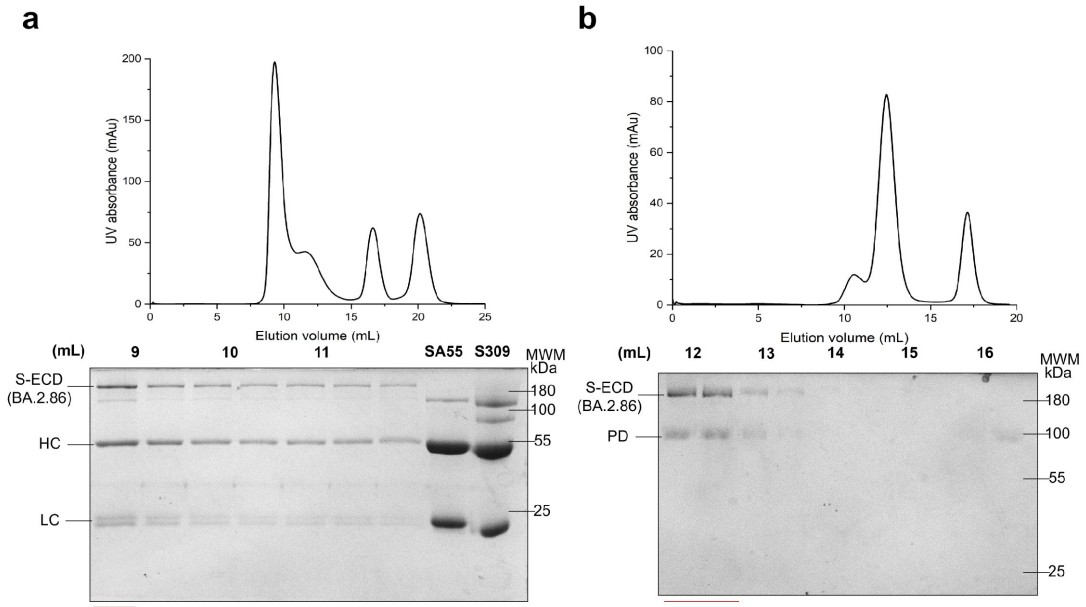

Representative SEC purification profile and fractions for cryo-EM analysis were marked by red line.

Fig. S5. SEC of ECD-ACE2 and ECD-IgG.

a. Representative SEC purification of the BA.2.86 ECD+PD. SDS–PAGE was visualized by Coomassie blue staining and fractions for cryo-EM analysis were marked by red line. **b**. Representative SEC purification of the BA.2.86 ECD+SA55+S309. SDS-PAGE was visualized by Coomassie blue staining and fractions for cryo-EM analysis were marked by red line. Source data are provided as a Source Data file.

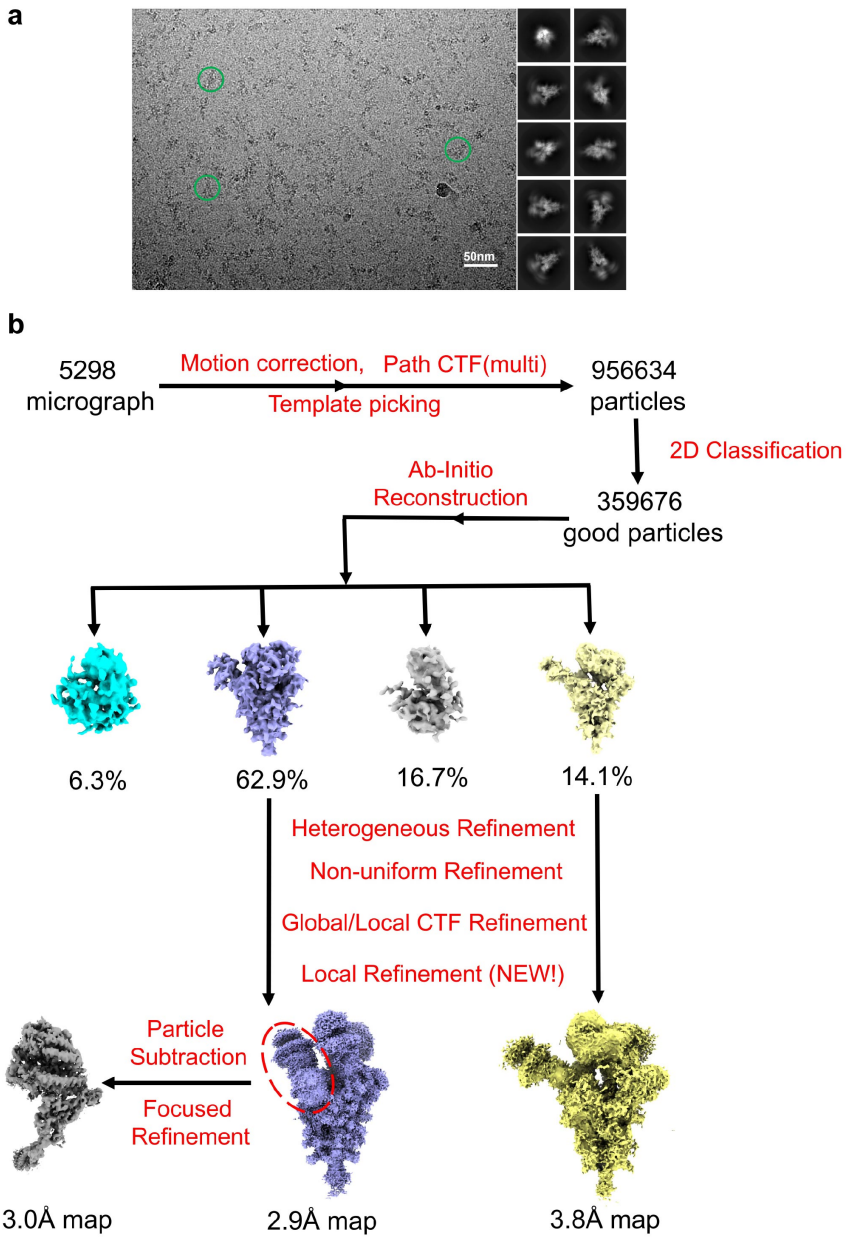

Fig. S6. Flowchart of BA.2.86-ACE2 for cryo-EM data processing.

a. Representative cryo-EM micrograph of BA.2.86-ACE2 complex particles. Green circles indicate selected particles. Scale bar: 50 nm. Insets show representative 2D class averages. **b**. Flowchart of the cryo-EM data processing. Starting with 5298 micrographs, particles are selected through motion correction and template picking, resulting in 956,634 particles. After 2D classification, 359,676 good particles are used for ab-initio reconstruction. Various refinement processes follow, leading to final 3D maps showing different particle populations: 6.3%, 62.9% (2.9 Å), 16.7%, and 14.1% (3.8 Å, a 'partially up' conformation). Key steps in the process are highlighted in red.

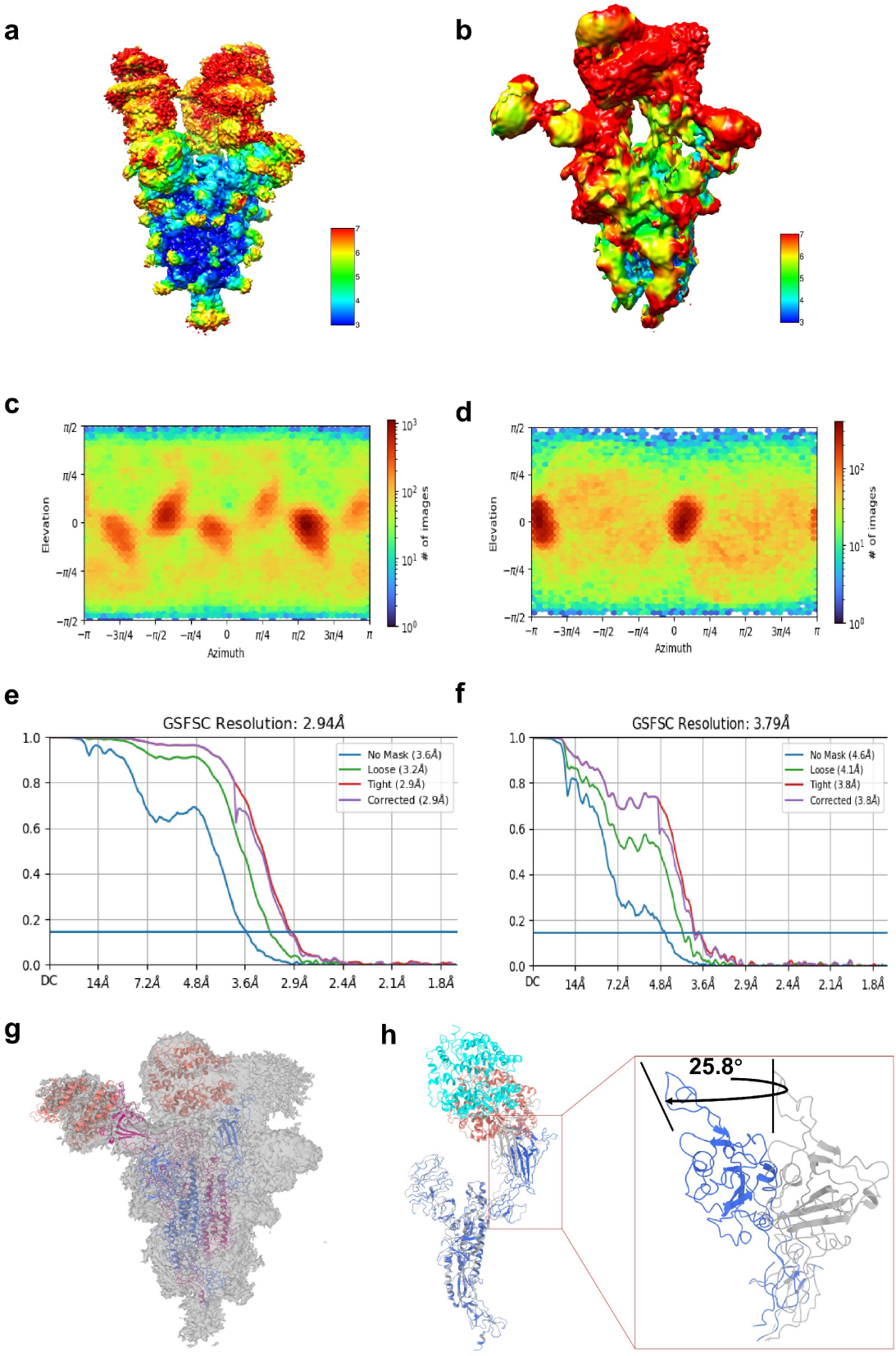

Fig. S7. Cryo-EM analysis of S-ECD from BA.2.86 with ACE2.

a, c and **e**, **a.** Local resolution map for the 3D reconstruction of the overall high-resolution structure. **c,** Euler angle distribution in the final 3D reconstruction of overall

map. **e,** FSC curve of the refined model of S-ECD (BA.2.86)-ACE2 versus the overall structure that it is refined against. **b, d** and **f**, **b.** Local resolution map for the 3D reconstruction of the overall other-conformation structure. **d,** Euler angle distribution in the final 3D reconstruction of overall map. **f,** FSC curve of the refined model of S-ECD (BA.2.86)-ACE2 versus the overall structure that it is refined against. **g-h.** BA.2.86 have other conformation relative to three up RBD, whose one RBD occurs tilt because of near ACE2 extrusion. Two panel are a view of the Spike-ACE2 interaction.

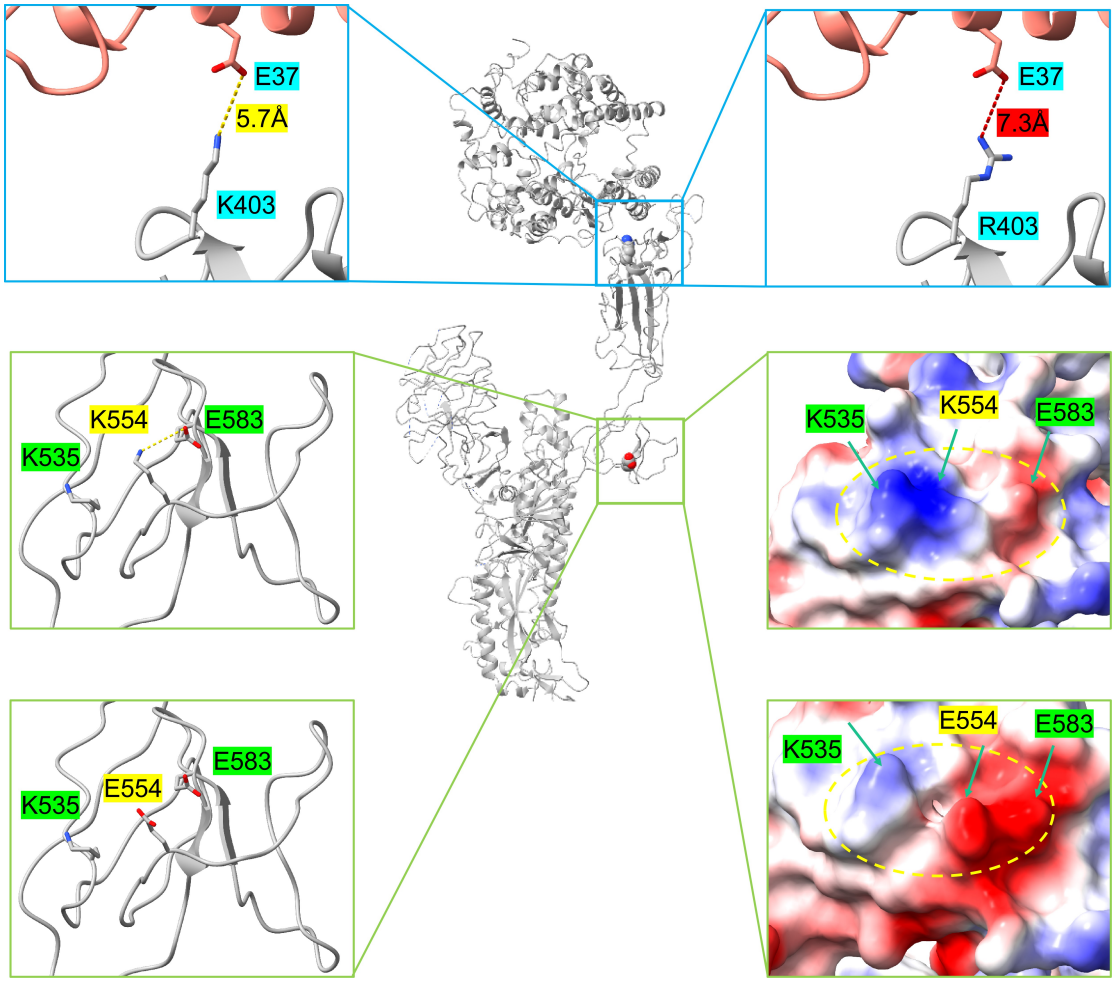

Fig. S8. Impact of E554K and R403K mutations on RBD-ACE2 interface.

The appearance of the partial 'up' conformation in the structure may be related to point mutations occurring at the E554K and R403K sites. The R403K is located in various region in the RBD-ACE2 interface. The distance between the 403 (RBD) and E37 (ACE2) changed from WT 7.3 Å to BA.2.86 5.7 Å, increasing the likelihood of ACE2 binding to RBD, and the red and yellow dashed lines represent distances only. The change of the 554 position from E to K alters the surrounding hydrogen bond interactions and electronic potential energy. Therefore, binding of ACE2 to RBD requires dissociation or breathing of the Spike trimer.

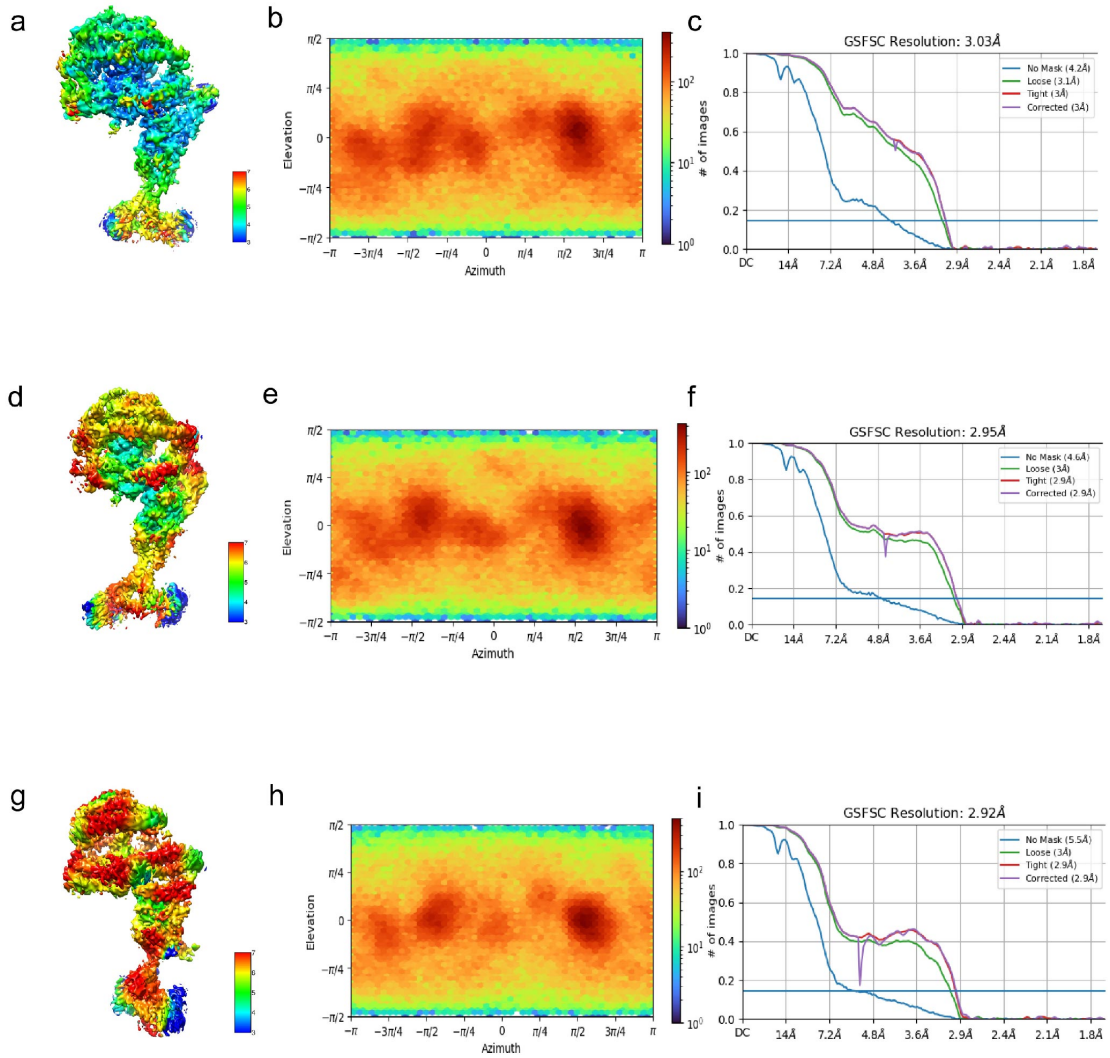

Fig. S9. Cryo-EM analysis of BA.2.86-RBD.

a, b and **c**, **a.** Local resolution map for the 3D reconstruction of the overall first RBD structure. **b,** Euler angle distribution in the final 3D reconstruction of overall map. **c,** FSC curve of the refined model of S-ECD (BA.2.86)-ACE2 versus the overall structure that it is refined against. **d, e** and **f**, **d.** Local resolution map for the 3D reconstruction of the overall second RBD structure. **e,** Euler angle distribution in the final 3D reconstruction of overall map. **f,** FSC curve of the refined model of S-ECD (BA.2.86)-ACE2 versus the overall structure that it is refined against. **g, h** and **i**, **g.** Local resolution map for the 3D reconstruction of the overall third RBD structure. **h,** Euler angle distribution in the final 3D reconstruction of overall map. **i,** FSC curve of the refined model of S-ECD (BA.2.86)-ACE2 versus the overall structure that it is refined against.

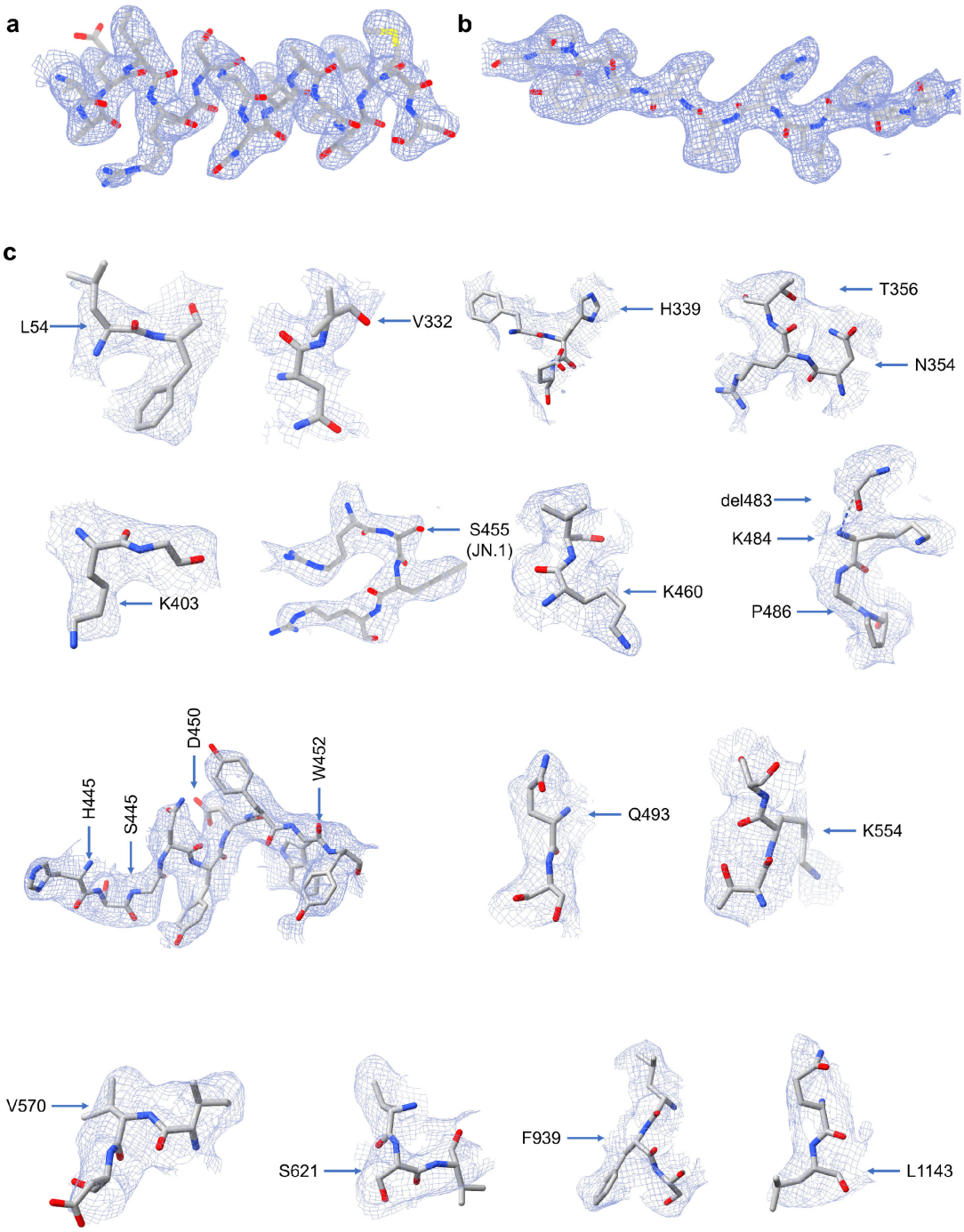

Fig. S10. Representative cryo-EM density maps.

a-b, Cryo-EM density map of BA.2.86-S-ECD is shown at threshold of 7 σ. **c**, The model of all 34 residues and S455 site (JN.1) with their density map is showed, other positions cannot be displayed due to poor density or excessive flexibility in the structure.

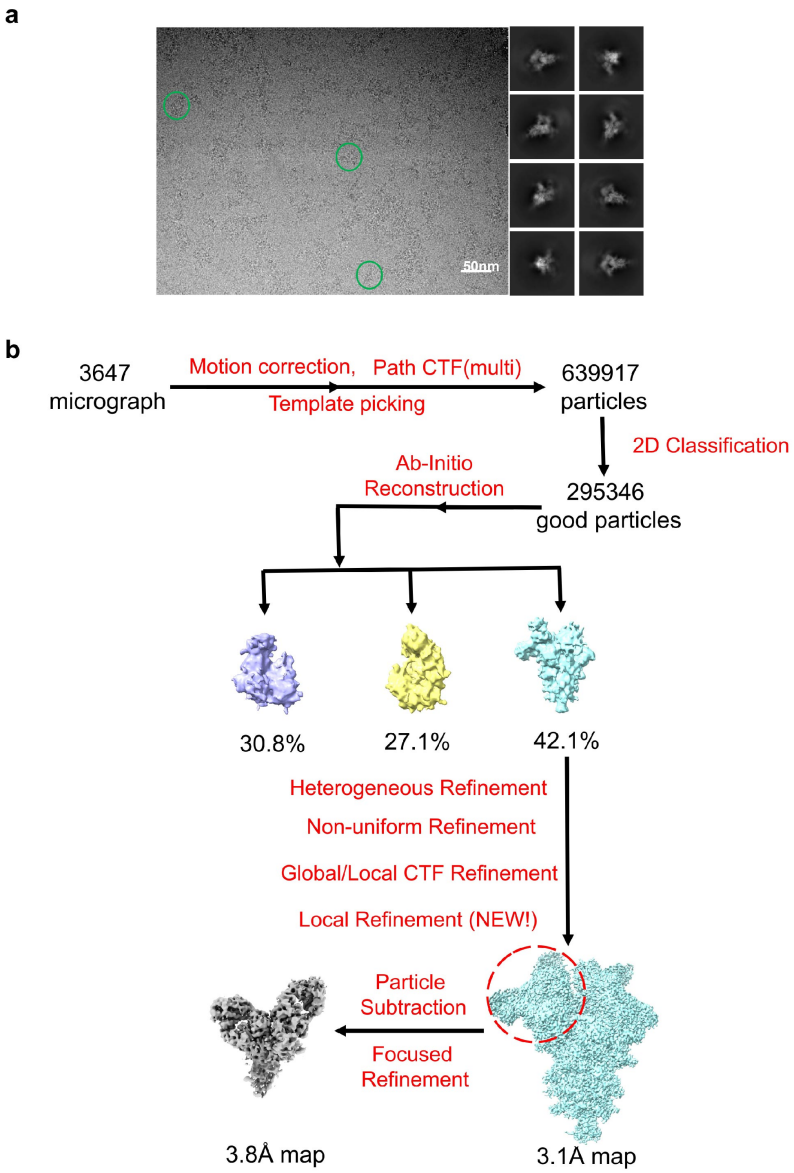

Fig. S11. Flowchart of BA.2.86-SA55-S309 for cryo-EM data processing.

a. Representative cryo-EM micrograph of BA.2.86-SA55-S309 complex particles. Green circles indicate selected particles. Scale bar: 50 nm. Insets show representative 2D class averages. **b**. Flowchart of the cryo-EM data processing. Starting with 3647 micrographs, particles are selected through motion correction and template picking, resulting in 639,917 particles. After 2D classification, 295,346 good particles are used for ab-initio reconstruction. Various refinement processes follow, leading to final 3D maps showing different particle populations: 30.8%, 27.1%, and 42.1% (3.1 Å). Key steps in the process are highlighted in red.

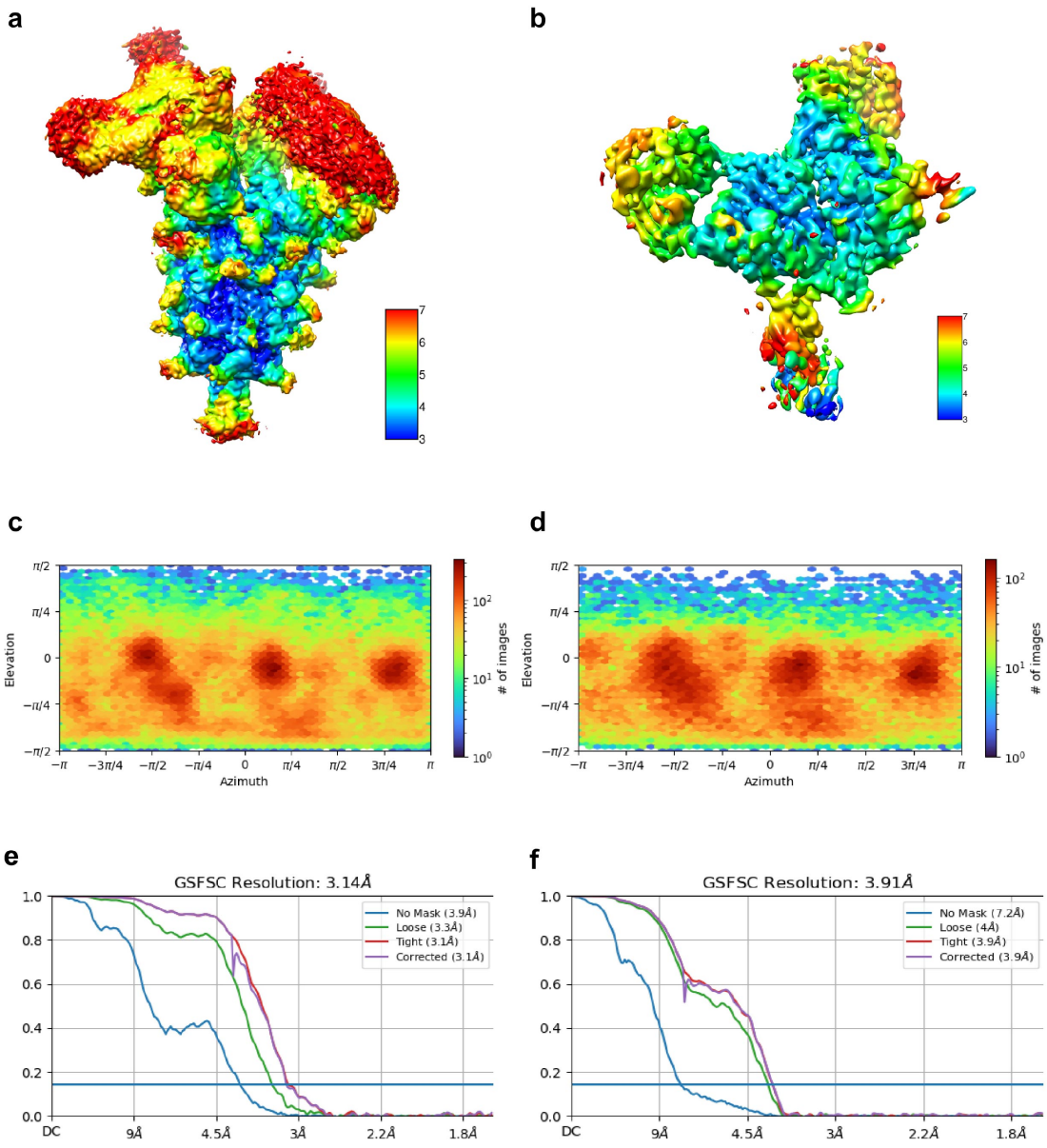

Fig. S12. Cryo-EM analysis of S from BA.2.86 with S309, SA55.

a, c and **e**, **a.** Local resolution map for the 3D reconstruction of the overall S-ECD with S309, SA55 structure. **c,** Euler angle distribution in the final 3D reconstruction of overall map. **e,** FSC curve of the refined model of S-ECD-S309-SA55 versus the overall structure that it is refined against. **b, d** and **f**, **b.** Local resolution map for the 3D reconstruction of the overall RBD with S309, SA55 structure. **d,** Euler angle distribution in the final 3D reconstruction of overall map. **f,** FSC curve of the refined model of RBD-S309-SA55 versus the overall structure that it is refined against.

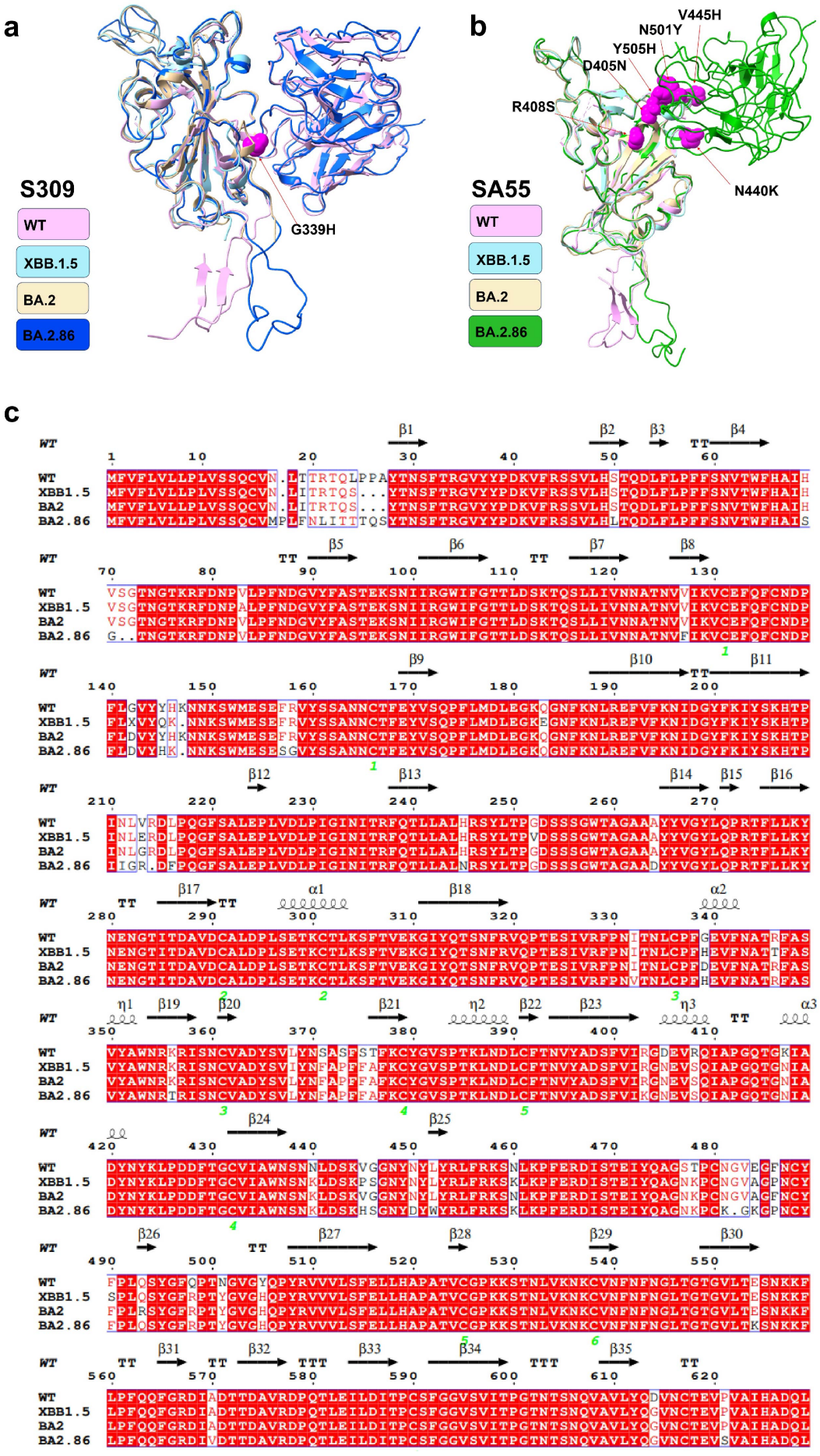
a
S309
WT
XBB.1.5
BA.2
BA.2.86
G339H
b
SA55
WT
XBB.1.5
BA.2
BA.2.86
V445H
N501Y
Y505H
D405N
R408S
N440K
c
WT
XBB1.5
BA2
BA2.86

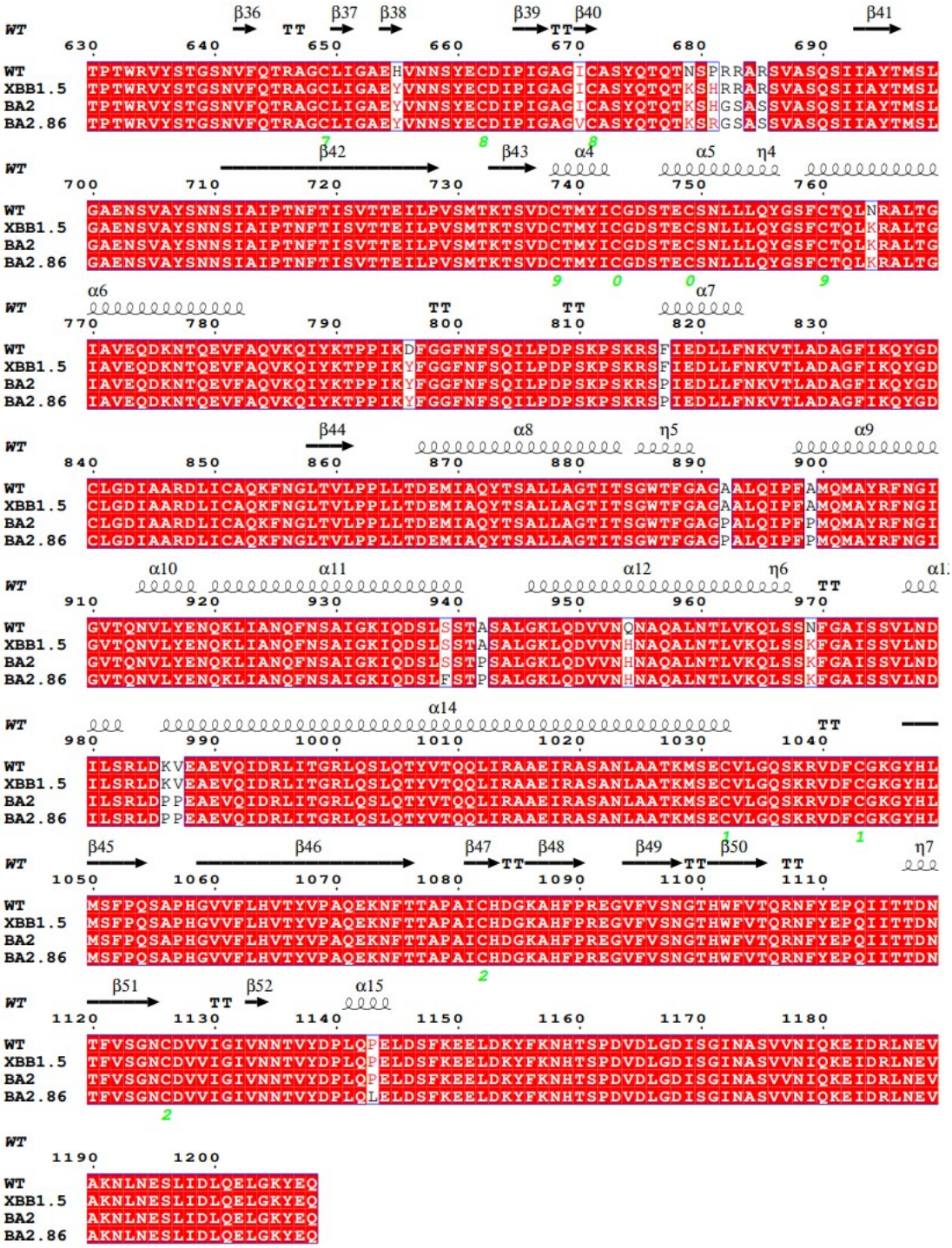

Fig. S13. Effect of RBD mutations on binding of S309 and SA55.

a-b. The binding epitope of S309 bound to the RBD and SA55 bound to the RBD are colored blue and green, which overlaps with the mutated residues (pink) relative to the BA.2-RBD on His336, His442, Ser443 and Asp447. **c**. Multiple sequence alignment of complete S-ECD of WT, XBB.1.5, BA.2, and BA.2.86 by CLUSTALW software.

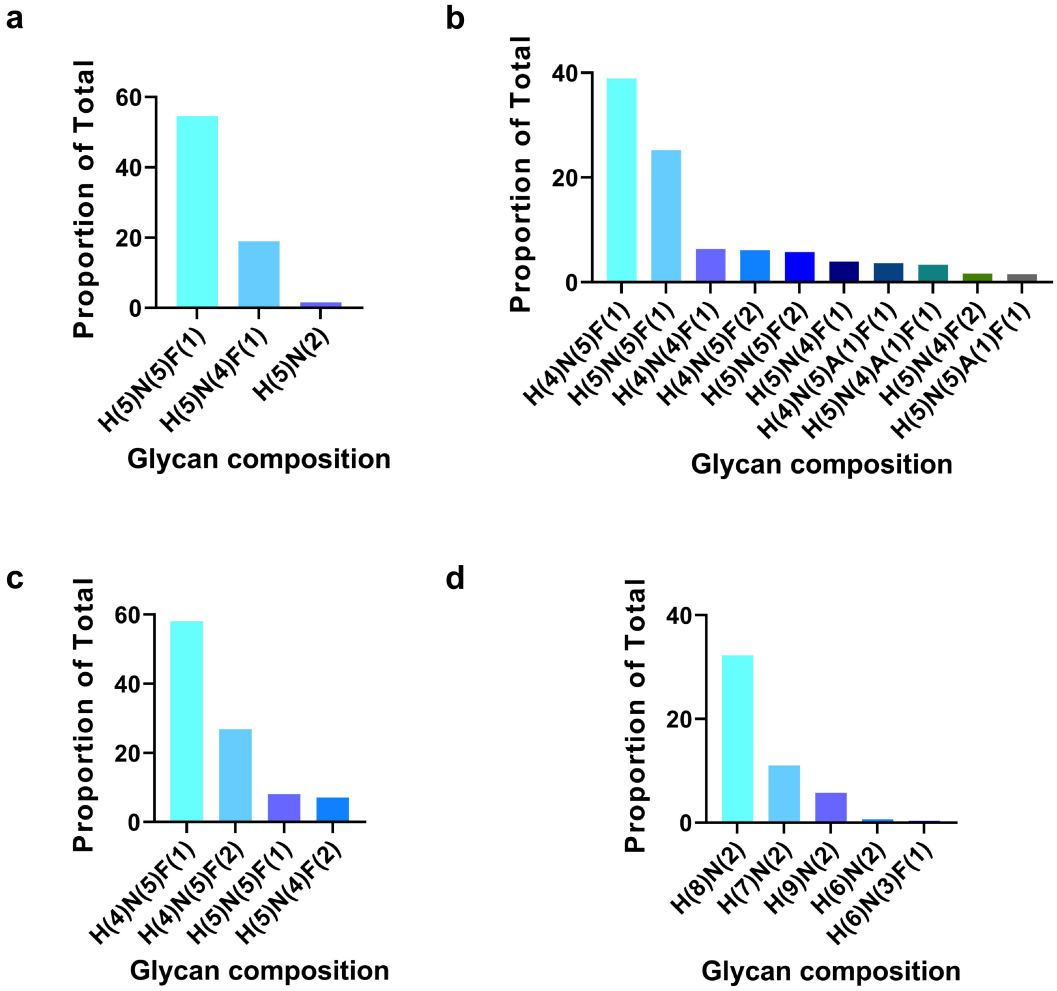

Fig. S14. Top ten glycan compositions that were identified at the sites Asn343 and Asn354 on S proteins of SARS-CoV-2.

a. Top ten glycan compositions that were identified at the site Asn343 of SARS-CoV-2 WT. **b.** Top ten glycan compositions that were identified at the site Asn343 of SARS-CoV-2 XBB.1.5. **c.** Top ten glycan compositions that were identified at the site Asn343 of SARS-CoV-2 BA.2.86. **d.** Top ten glycan compositions that were identified at the site Asn354 of SARS-CoV-2 BA.2.86. H represents hexose; N represents N-acetylglucosamine; F represents fucose; A represents sialic acid. Data were analyzed with GraphPad 9.0 software. Source data are provided as a Source Data file.

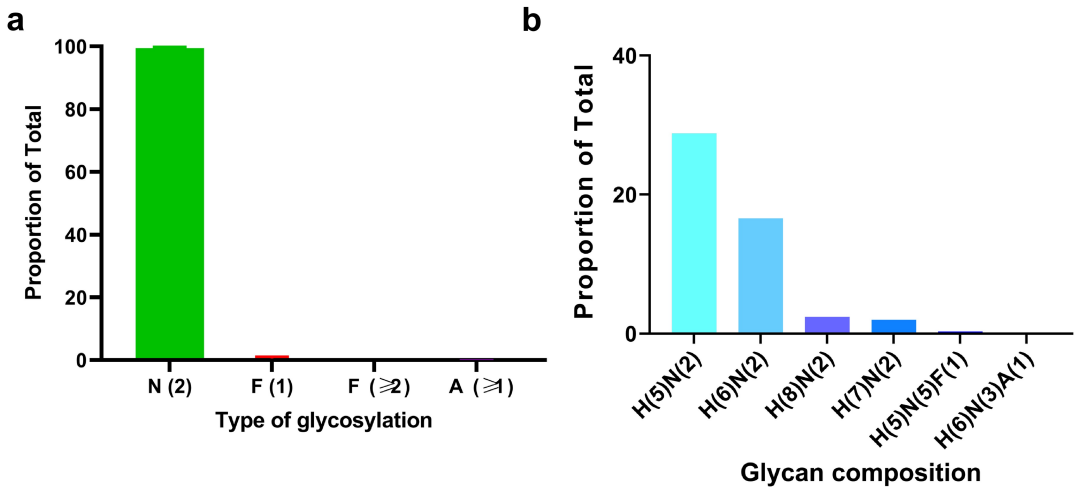

Fig. S15. N-linked glycosylation profile of the site Asn245 of SARS-CoV-2 BA.2.86. **a.** N-linked glycosylation profile of the site Asn245 that was identified from S protein of SARS-CoV-2 BA.2.86. **b.** Top ten glycan compositions that were identified at the site Asn245 of SARS-CoV-2 BA.2.86. N-linked glycans were divided into four basic classifications, including high mannose glycosylation (N2), mono-fucosylation (F1), multi-fucosylation (with ⩾ 2 fucose residues, F ⩾ 2), and sialylation (A ⩾ 1). H represents hexose, N represents N-acetylglucosamine, F represents fucose, A represents sialic acid. Source data are provided as a Source Data file.

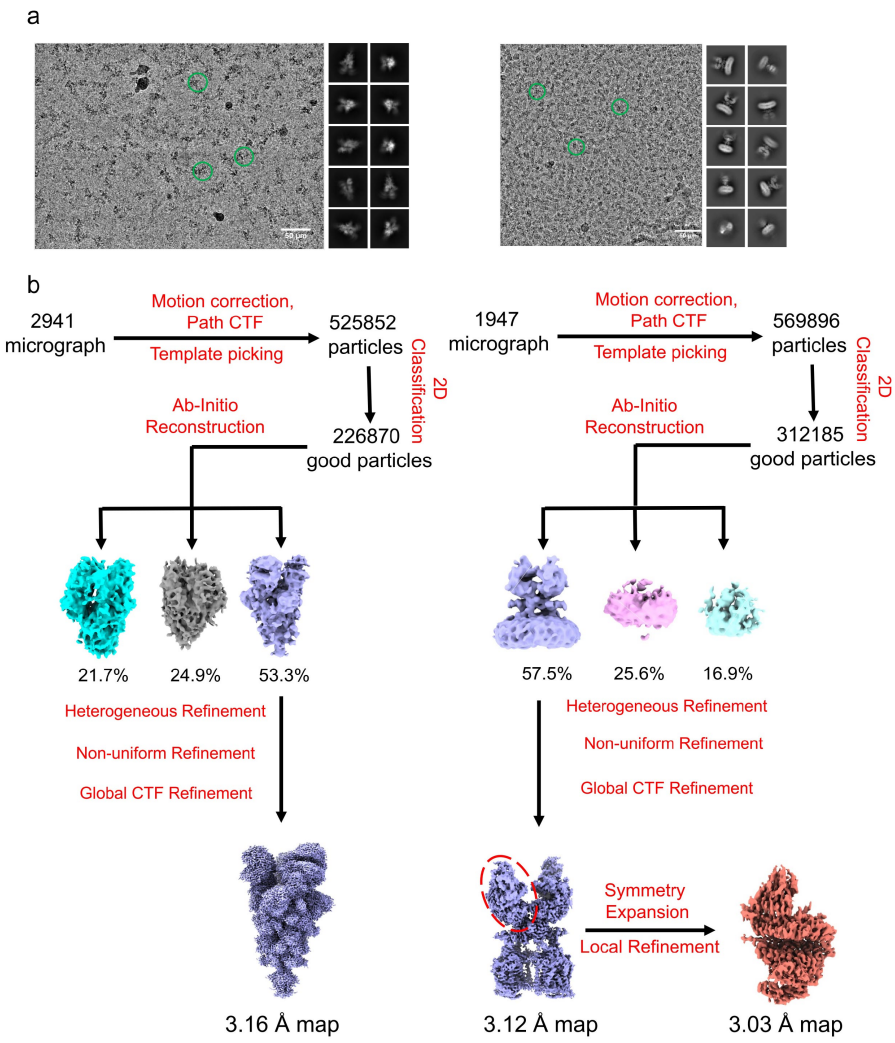

Fig. S16. Flowchart of JN.1-Spike and JN.1 RBD-SLC6A19-ACE2 for cryo-EM data processing.

a. Representative cryo-EM micrographs of JN.1-Spike (left) and JN.1 RBD-SLC6A19-ACE2 complex particles (right). Green circles indicate selected particles. Scale bar: 50 nm. Insets show representative 2D class averages. **b**. Flowchart of cryo-EM data processing. For JN.1-Spike (left): Starting with 2941 micrographs, 525,852 particles were selected, and 226,870 good particles were used for ab-initio reconstruction. Final 3D maps show particle populations of 21.7%, 24.9%, and 53.3% (3.16 Å resolution). For JN.1 RBD-SLC6A19-ACE2 (right): Starting with 1947 micrographs, 569,896 particles were selected, and 312,185 good particles were used for ab-initio reconstruction. Final 3D maps show particle populations of 57.5%, 25.6%, and 16.9% (3.12 Å). Key steps are highlighted in red.

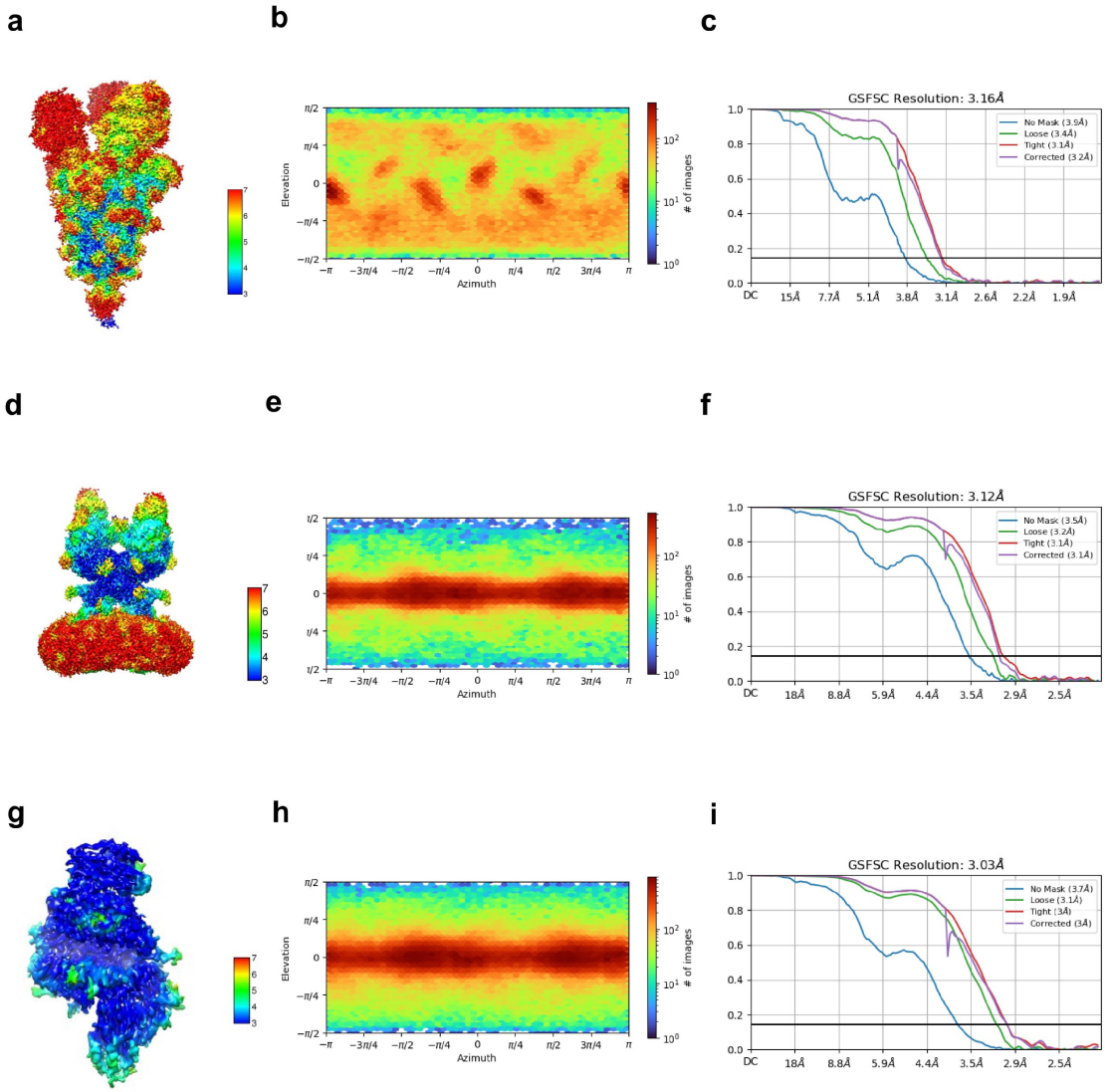

Fig. S17. Cryo-EM analysis of JN.1-Spike-PD and JN.1 RBD-SLC6A19-ACE2.

a, b and **c**, **a.** Global resolution map for the 3D reconstruction of the overall Spike structure. **b,** Euler angle distribution in the final 3D reconstruction of overall map. **c,** FSC curve of the refined model of S-ECD (JN.1)-ACE2 versus the overall structure that it is refined against. **d, e** and **f**, **d.** Local resolution map for the 3D reconstruction of the overall second RBD structure. **e,** Euler angle distribution in the final 3D reconstruction of overall map. **f,** FSC curve of the refined model of JN.1 RBD-SLC6A19-ACE2 versus the overall structure that it is refined against. **g, h** and **i**, **g.** Local resolution map for the 3D reconstruction of the overall JN.1 RBD-SLC6A19-ACE2 structure. **h,** Euler angle distribution in the final 3D reconstruction of overall map. **i,** FSC curve of the refined model of JN.1 RBD-SLC6A19-ACE2 versus the overall structure that it is refined against.

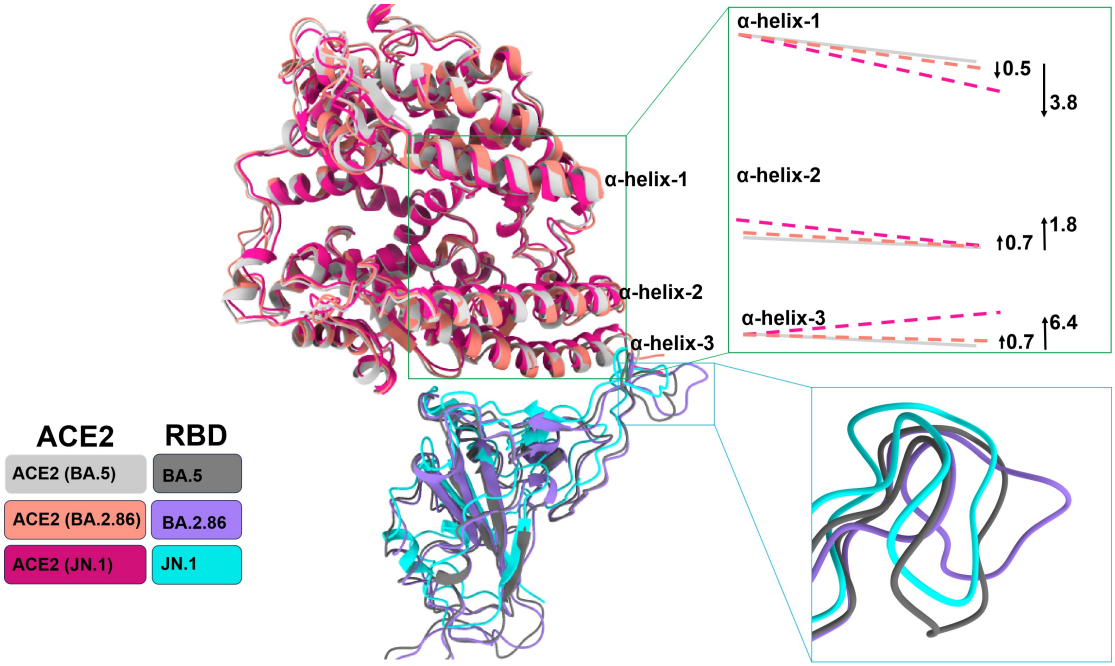

Fig. S18. L455S tilts the three α-helix of ACE2 adjacent to the RBD region.

L455S tilts the three α-helix of ACE2 adjacent to the RBD region as visualized by overlay of BA.5-RBD-ACE2, BA.2.86-RBD-ACE2 and JN.1-RBD-ACE2. Meanwhile, compared with BA.2.86, JN.1 showed a significant shift in tips.

Table S1. Cryo-EM data collection, refinement and validation statistics.

Data collection		
EM equipment	Titan Krios	Titan Krios
Voltage (kV)	300	300
Detector	Gatan K3 Summit	Gatan K3 Summit
Energy filter	Gatan GIF Quantum	Gatan GIF Quantum
Pixel size (Å)	0.855	0.83
Electron dose (e-/Å2)	50	50
Defocus range (μm)	-1.1 ~ -1.6	-1.1 ~ -1.6
Sample	BA.2.86-ECD-ACE2	BA.2.86-ECD-S309-SA55
Number of collected micrographs	5,298	3,647
3D Reconstruction		
Software	cryoSPARC	cryoSPARC
Sample	Overall	Overall
Number of used particles	226,236	124,340
Resolution (Å)	2.9	3.1
Symmetry	C1	C1
Map sharpening B-factor (Å2)	-90	-90
Refinement		
Software	cryoSPARC	cryoSPARC
Protein residues	5,415	5,040
Side chains assigned	5,415	5,040
Sugar	74	74
R.m.s deviations		
Bonds length (Å)	0.01	0.019
Bonds Angle (°)	0.908	0.920
Validation		
Clash score	8.62	6.34
rotamer outliers (%)	0.07	3.08
Ramachandran plot statistics (%)		
Favored	90.18	91.17
Allowed	9.00	8.43
Outlier	0.82	1.27

Table S2. The epitopes of five broadly neutralizing mAbs.

	SA55	S309	COVOX-45	N-612-056	S2K146
	PDB:8WYJ	PDB:8WYJ	PDB:7PRY	PDB:7S0B	PDB:7TAT
333		P			
334		P			
335		P			
336		P			
337		P			
339		P			
340		P			
341		P			
343		P			
344		P			
345		P			
346		P		P	
348				P	
351				P	
352				P	
353			P	P	
354		P	P	P	
355			P	P	
356		P	P	P	
357		P	P	P	
358		P			
359			P		
360			P		
361		P			
375	P				
376	P				
394			P		
396			P	P	
403	P				
404	P				
405	P				
406	P				
407	P				
408	P				
417					P
426			P		
428			P		
437	P				
439	P				
440	P	P			
441		P			
445	P				
449					P
455					P
456					P

457				P	
459				P	
460				P	
462			P	P	
463			P		
464			P	P	
465			P	P	
466			P	P	
467				P	
468			P	P	
469				P	
471				P	
475					P
476					P
484					P
485					P
486					P
487					P
489					P
490					P
492					P
493					P
494					P
496					P
497					P
498	P				P
499	P				
500	P				
501	P				P
502	P				P
503	P				
504	P				
505	P				P
509		P			
516			P		
518			P		
519			P		
520			P		
521			P		
523			P		

P indicates the mAb recognizes RBD antigenic sites.

Table S3. Cryo-EM data collection, refinement and validation statistics.

Data collection	
EM equipment	Titan Krios
Voltage (kV)	300
Detector	Gatan K3 Summit
Energy filter	Gatan GIF Quantum
Pixel size (Å)	1.1
Electron dose (e-/Å2)	50
Defocus range (μm)	-1.2 ~ -1.6
Sample	JN.1 RBD-B^0AT1-ACE2
Number of collected micrographs	1,947
3D Reconstruction	
Software	cryoSPARC
Sample	Overall
Number of used particles	312,185
Resolution (Å)	3.12
Symmetry	C2
Map sharpening B-factor (Å2)	-90
Refinement	
Software	cryoSPARC
Protein residues	932
Side chains assigned	
Sugar	0
R.m.s deviations	
Bonds length (Å)	0.003
Bonds Angle (°)	0.751
Validation	
Clash score	23
rotamer outliers (%)	0
Ramachandran plot statistics (%)	
Favored	85.42
Allowed	14.58
Outlier	0